

# Catalysis Science & Technology

Accepted Manuscript

View Article Online  
View Journal

This article can be cited before page numbers have been issued, to do this please use: S. Kumar, M. M. Devi, S. Kansal and S. Saravanamurugan, *Catal. Sci. Technol.*, 2020, DOI: 10.1039/D0CY01259A.



This is an Accepted Manuscript, which has been through the Royal Society of Chemistry peer review process and has been accepted for publication.

Accepted Manuscripts are published online shortly after acceptance, before technical editing, formatting and proof reading. Using this free service, authors can make their results available to the community, in citable form, before we publish the edited article. We will replace this Accepted Manuscript with the edited and formatted Advance Article as soon as it is available.

You can find more information about Accepted Manuscripts in the [Information for Authors](#).

Please note that technical editing may introduce minor changes to the text and/or graphics, which may alter content. The journal's standard [Terms & Conditions](#) and the [Ethical guidelines](#) still apply. In no event shall the Royal Society of Chemistry be held responsible for any errors or omissions in this Accepted Manuscript or any consequences arising from the use of any information it contains.

## ARTICLE

# Untangling the Active Sites in Exposed Crystal Facet of Zirconium Oxide for Selective Hydrogenation of Bioaldehydes

Sahil Kumar<sup>a</sup>, Mayanglambam Manolata Devi<sup>a</sup>, Sushil Kumar Kansal<sup>b</sup>, Shunmugavel Saravanamurugan<sup>\*a</sup>

Received 00th January 20xx,  
Accepted 00th January 20xx

DOI: 10.1039/x0xx00000x

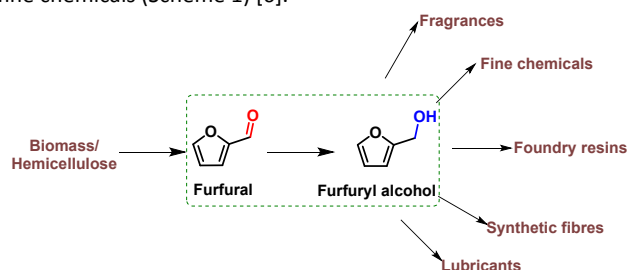
The present study reports the influence of crystal phase, facets, and the active sites of zirconium oxide (ZrO<sub>2</sub>) on the conversion of bio-aldehydes to corresponding alcohols in isopropanol under mild reaction condition. Various ZrO<sub>2</sub>-based catalysts, having a different composition of monoclinic and tetragonal crystal phases, are successfully prepared in the presence of a base via the solvothermal process. From the detailed characterizations through XRD, TEM, CO<sub>2</sub>-TPD, XPS, AES, BET and poisoning studies, M-ZrO<sub>2</sub>-U-N, synthesized using zirconium oxynitrate and urea as precursor and precipitant, respectively, in water, possesses 100% monoclinic crystal phase with a maximum amount of exposed (-111) facet and surface oxygen concentration along with the highest number of basic sites. The catalytic study on the transformation of furfural (FFA) to furfuryl alcohol (FOH) reveals that M-ZrO<sub>2</sub>-U-N exhibits the best efficiency with a nearly quantitative yield of FOH. On the other hand, T-ZrO<sub>2</sub>-U-N, synthesized using zirconium oxynitrate and urea as precursor and precipitant, respectively, in methanol, is found to have 94.4% tetragonal phase and 2.2-fold lower basic sites in comparison with that of M-ZrO<sub>2</sub>-U-N. The catalytic result with T-ZrO<sub>2</sub>-U-N displays the lowest activity in terms of FOH yield (8.1%). According to comparative and systematic catalytic studies with the various ZrO<sub>2</sub> catalysts having a different amount of tetragonal and monoclinic phases, the ZrO<sub>2</sub> having more monoclinic phase with more exposed (-111) facet, basic sites, surface oxygen species and surface area is found to be crucial for the FFA conversion to FOH with high selectivity. M-ZrO<sub>2</sub>-U-N is found to be stable, recyclable and also shows excellent activity towards the transformation of other bio-aldehydes and ketones to their corresponding alcohols.

**Keywords:** Furfural, Hydrogenation, Furfuryl alcohol, ZrO<sub>2</sub>, Monoclinic, Crystal phase and facet, Basic sites

## 1. Introduction

Societal needs of energy, fuels and chemicals have been continuously fulfilled by the outputs based on fossil resources. However, the anticipation of diminishing the confined resources of fossils in the future accentuates the essential need for sustainable resources [1]. With regard to this, terrestrial lignocellulosic biomass is deemed as an alternative sustainable resource with high abundant in nature as a source of carbon, which can potentially replace the chemicals derived from fossil resources. The oxygen-rich lignocellulosic biomass with intertwined structure can be transformed to high-value chemicals through various processes, such as dehydration, hydrogenation and hydrodeoxygenation [2]. Of which, hydrogenation process is one of the most useful transformations for producing several benchmark chemicals with a wide range of applications including pharmaceuticals, agrochemicals and fine chemicals [3]. Most platform chemicals derived from biomass contain more than one unsaturated functional group, especially aromatic compounds having carbonyl groups such as furfural (FFA)

and 5-hydroxymethylfurfural (HMF). FFA is regarded as one of the top value-added chemicals, which can be used as a starting substrate for producing a broad spectrum of chemicals like, e.g., alcohols, hydrocarbons and biofuels [4]. However, the catalytically selective transformation of such molecules having multi-functionalities to target products under benign reaction conditions is still a challenge. Thus, the catalysts having a unique activity to selectively produce the target product by preventing the formation of undesired products has significantly become appealing [5]. In connection with this, the selective hydrogenation of FFA to furfuryl alcohol (FOH) is considered to be one of the important transformations as FOH has extensive applications in foundry resins, synthetic fibres, lubricants and other fine chemicals (Scheme 1) [6].



Scheme 1. Hydrogenation of furfural to furfuryl alcohol and its applications.

<sup>a</sup>Laboratory of bioproduct chemistry, Center of Innovative and Applied Bioprocessing, Sector-81 (Knowledge City), Mohali - 140 306, Punjab, India. Email: saravana@ciab.res.in

<sup>b</sup>Dr. S. S. Bhatnagar University Institute of Chemical Engineering and Technology, Panjab University, Chandigarh, 160 014, India.

Importantly, 62.0% total annual production of FFA is being converted into FOH every year to meet the demands in the polymer industry [7]. Copper chromite catalyst is currently being used for commercial production of FOH from FFA in the liquid phase reaction; however, the toxicity and lower stability associated with chromium metal makes this catalyst system perilous to the environment [8]. To overcome these significant drawbacks, various noble and non-noble metal-based catalysts based on Ir, Pd, Pt, Ru, Cu and Ni have been explored, yielding 90.0 – 99.0% of FOH [9-15]. In addition to this, some bimetallic catalysts, such as Cu-MgO, Pt-Sn, Ni-Sn, Ru-Sn, Pt-Co and Pd-Ru were also reported for the conversion of FFA to FOH under high hydrogen pressure reaction condition, achieving very high selectivity of FOH [16-21]. However, the studies mentioned above also have drawbacks such as performing reactions at relatively high temperature, pressure, the requirement of a highly sophisticated instrument(s), accumulation/sintering of particles and leaching of metal(s), thus decreasing the activity and stability of the catalyst(s) in the subsequent runs.

Hydrosilane-mediated hydrogenation of FFA was also studied over Pd/C under very mild conditions, yielding excellent FOH selectivity (>99%) [22], but the separation of the product after the reaction is a challenging task. Catalytic transfer hydrogenation (CTH) is an alternative approach in which organic compounds, such as formic acid and isopropanol, were employed as in situ H-donor [23]. In line with this, Ahn et al. performed FFA hydrogenation with Rh/ED-KIT-6 using formic acid as H-donor in isopropanol, affording 98.0% yield of FOH [8]. Instead of using organic acid, alcohols are preferred for CTH reaction as they play a dual role as solvent and H-donor. CTH reaction generally involves through Meerwein-Ponndorf-Verley (MPV) reduction mechanism, in which the carbonyl group of the compound gets reduced to the respective alcohol [24]. Marchi et al. reported FFA hydrogenation with Cu-Mg-Al (40 wt. % Cu) as a catalyst in isopropanol at 150 °C, giving a quantitative yield of FOH [25]. Although a quantitative yield FOH obtained, the catalytic system was found unappealing due to a high content of copper loading. Al-Zr@Fe and commercial NiO were also reported for the conversion of FFA to FOH in isopropanol at 170-180 °C, achieving 90.4 and 94.0% of FOH, respectively [26, 27]. Hydrotalcite derived mixed oxide catalyst have also been employed as catalysts for the transformation of FFA, attaining a high selectivity (97.0%) at 110 °C, 30 bar H<sub>2</sub> pressure [28]. Co<sub>3</sub>O<sub>4</sub>-Al<sub>2</sub>O<sub>3</sub> over hydrotalcite supported catalyst also offered FOH selectivity of 92% at 180 °C [29]. In a nutshell, the studies above related to FFA hydrogenation indicate the uses of harsh reaction conditions along with toxic metal(s) such as chromium and precious metal(s) as catalysts, showing the inevitability for designing robust catalyst.

Catalysts containing metal oxides/metal hydroxides without other auxiliary metal(s) have also been recently reported for the upgradation of biomass-derived substrates [30, 31]. Among the reported various metal oxides, ZrO<sub>2</sub> is found to be promising due to its tuneable acidic and basic properties along with high hydrothermal stability [32]. In connection with this, the organophosphate group incorporated in ZrO<sub>2</sub> and nanohybrid ZrO<sub>2</sub> were reported for the transformation of FFA to FOH in isopropanol. The role of incorporating organophosphate group was to introduce bifunctional acidic and basic sites in ZrO<sub>2</sub>, resulting in a near-quantitative yield of

FOH (98.0%) [33]. FDCA-based zirconium hybrid prepared by a hydrothermal treatment was also applied for FFA hydrogenation to FOH (96.0%) [34]. High loading of zirconium carbonate as catalyst was also studied, achieving 99% FOH from FFA [35]. The use of these organic molecules for generating active sites has a complicated synthetic procedure and no high thermal stability. In this context, Zhang et al. prepared amorphous zirconium hydroxide by using ammonia as a precipitating agent and tested for FFA hydrogenation to FOH (98%) under relatively high temperature (170 °C) at 10 bar of nitrogen pressure [36]. The XRD results showed that zirconium hydroxide possessed an amorphous structure, suggesting the requirement of highly stable, crystalline material. Li et al. found a single-phase monoclinic, and tetragonal zirconium oxide prepared using a hydrothermal and solvothermal treatment in water and methanol as solvent, respectively [37]. This pioneering work provoked us to explore the role of crystal phase and exposed facet of ZrO<sub>2</sub> on the hydrogenation of FFA to FOH in isopropanol.

Here, we report the synthesis of a series of ZrO<sub>2</sub> possessing various composition of monoclinic and tetragonal phases in methanol/water by the solvothermal approach in the presence of a base as precipitant. All the synthesized catalysts were characterized with XRD, Raman, HRTEM, CO<sub>2</sub>-TPD, XPS, AES, and BET and investigated for the catalytic transformation of FFA to FOH under identical reaction conditions in isopropanol. The optimisation of various reaction parameters, kinetic study and recyclability of the best performing catalyst (M-ZrO<sub>2</sub>-U-N) were also performed. Moreover, the present study focuses on exploring the role of crystal phase, and facet, active site and surface oxygen concentration of ZrO<sub>2</sub> on the yield of FOH as no report related to these aspects have been disclosed so far to the best of our knowledge.

## 2. Results and Discussion

### 2.1 Catalytic Activities of ZrO<sub>2</sub>

The synthesized ZrO<sub>2</sub> catalysts were employed for the transformation of FFA to FOH in isopropanol at 110 °C and the results are summarised in Table 1. ZrO<sub>2</sub>, synthesized by using zirconium oxychloride and zirconium oxynitrate as precursors and urea as a precipitant in water (designated as M-ZrO<sub>2</sub>-U-C and M-ZrO<sub>2</sub>-U-N), showed excellent activity, giving maximum yield of 85.5 and 89.8% FOH, respectively (Table 1, entry 1 and 3). On the other hand, the similarly prepared ZrO<sub>2</sub> in methanol instead of water as a solvent (T-ZrO<sub>2</sub>-U-C and T-ZrO<sub>2</sub>-U-N) (Table 1, entry 2 and 4) exhibited inferior catalytic activity, affording 34.2 and 8.1% FOH, respectively. For comparison, the catalytic activity of the commercially available ZrO<sub>2</sub> (ZrO<sub>2</sub>-C) prepared by simply calcination of zirconium oxide at 400 °C was also employed as catalysts. The obtained results revealed that ZrO<sub>2</sub>-C gave a negligible yield of FOH (<1.0%) along with difurfuryl ether as a major product, confirmed by GC-MS (Table 1, entry 5). From Table 1, one can understand that ZrO<sub>2</sub> synthesised with two different precursors in the presence of urea as precipitant in water displayed an excellent catalytic activity than other ZrO<sub>2</sub> catalysts, intriguing to get a deeper understanding into the physicochemical properties of the ZrO<sub>2</sub> materials.

Table 1: Screening of various  $\text{ZrO}_2$  catalysts for furfural hydrogenation in isopropanol.

Entry	Catalyst	FFA Conv. (%)	FOH Yield (%)	FOH Sel. (%)
1	M-ZrO <sub>2</sub> -U-C	92.0	85.5	92.9
2	T-ZrO <sub>2</sub> -U-C	44.7	34.2	76.5
3	M-ZrO <sub>2</sub> -U-N	92.4	89.8	97.1
4	T-ZrO <sub>2</sub> -U-N	22.2	8.1	36.4
5	ZrO <sub>2</sub> -C	10.9	0.72	6.6

Reaction Conditions: 1 mmol FFA, 80 mg Catalyst, 4 mL Isopropanol, 110 °C, 6 h.

## 2.2 Influence of crystal phase on the catalytic activity

**XRD Analysis:** In order to understand the diverse activities of the  $\text{ZrO}_2$  catalysts, the crystal phases and purity of all the  $\text{ZrO}_2$  catalysts were analysed with X-ray diffractometer. The characteristic XRD patterns of the most and least efficient catalysts (M-ZrO<sub>2</sub>-U-N and T-ZrO<sub>2</sub>-U-N) are shown in Figure 1. The XRD pattern of M-ZrO<sub>2</sub>-U-N exhibited peaks corresponding to the crystal facets of (110), (-111), (111), (200), (-112) and (211) of the monoclinic phase of  $\text{ZrO}_2$  according to JCPDS no. 00-037-1484. No other peak corresponding to any unreacted reagents was observed, inferring that M-ZrO<sub>2</sub>-U-N is purely composed of monoclinic  $\text{ZrO}_2$ . Whereas, the XRD pattern of T-ZrO<sub>2</sub>-U-N displayed diffraction peaks at  $2\theta$  of 30.2, 35.3, 50.3, 59.7 and 73.9, which can be indexed to the corresponding crystal facets of (111), (200), (220), (311) and (400) of tetragonal phase of  $\text{ZrO}_2$  (JCPDS # 00-017-0923). On careful observation, the maximum intensity of (111) peak of T-ZrO<sub>2</sub>-U-N does not seem to be symmetrical in shape; thus, the peak was deconvoluted and is shown in an inset in Figure 1. The deconvoluted pattern showed two peaks corresponding to a minor and major peak of (-111) plane of monoclinic and (111) plane of tetragonal  $\text{ZrO}_2$ , respectively, implying that T-ZrO<sub>2</sub>-U-N catalyst composed of both monoclinic as well as tetragonal phases.

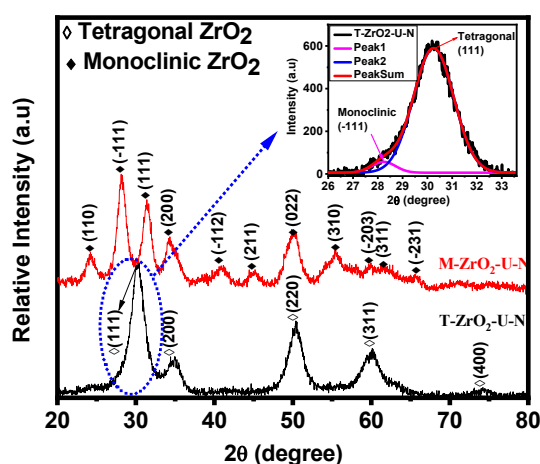


Figure 1. X-ray diffraction patterns of M-ZrO<sub>2</sub>-U-N and T-ZrO<sub>2</sub>-U-N. The inset shows deconvoluted (111) peak of T-ZrO<sub>2</sub>-U-N.

The amount of monoclinic was found to be only 5.6% (Table S1). From these observations, one can understand that M-ZrO<sub>2</sub>-U-N exclusively composed of pure monoclinic phase exhibited the best catalytic efficiency (89.8% FOH). Whereas T-ZrO<sub>2</sub>-U-N having composed of tetragonal (94.4%) and monoclinic (5.6%) phase displayed a minimal catalytic activity (8.1% FOH), substantiating the prominent catalytic role of the monoclinic phase in  $\text{ZrO}_2$  under given reaction condition. The XRD patterns and the composition of tetragonal and monoclinic phases of other  $\text{ZrO}_2$  catalysts are shown in Figure S1 and Table S1, respectively. The detailed XRD analysis revealed a similar trend in terms of catalytic activity that the higher the fraction of monoclinic phase composition, the higher the yield of FOH. However, M-ZrO<sub>2</sub>-U-C and M-ZrO<sub>2</sub>-U-N, having the same content of monoclinic phase (100%), showed FOH selectivity of 92.9 and 97.1, respectively (Table 1 and S1). This discrepancy in the catalytic activity of M-ZrO<sub>2</sub>-U-C and M-ZrO<sub>2</sub>-U-N could be explained based on the relative ratio of crystal facets between (-111) and (111). M-ZrO<sub>2</sub>-U-N possessed a ratio of 1.51 while M-ZrO<sub>2</sub>-U-C had a slightly lower ratio of 1.44 respectively, inferring that (-111) crystal facet might have played a significant role in enhancing the yield of FOH [38] (Table S2).

**Raman Analysis:** To further substantiate the presence of monoclinic and tetragonal phases in  $\text{ZrO}_2$  catalysts, M-ZrO<sub>2</sub>-U-N and T-ZrO<sub>2</sub>-U-N were analysed with complementary technique Raman spectroscopy, and the obtained Raman spectra are shown in Figure S2. The Raman spectrum of M-ZrO<sub>2</sub>-U-N showed characteristic peaks at 182, 222, 306, 341, 382, 479, 540, 559 and 618  $\text{cm}^{-1}$ , which could be ascribed to the monoclinic phase of  $\text{ZrO}_2$  [37]. Likewise, T-ZrO<sub>2</sub>-U-N displayed peaks at 222, 274, 327, 382, 462, 475, 556, 621, and 644  $\text{cm}^{-1}$ . Of which, the peaks at 274, 327, 462, 475, 556, 621, and 644  $\text{cm}^{-1}$  can be assigned to the tetragonal phase of  $\text{ZrO}_2$ ; however, the peaks at 222 and 382  $\text{cm}^{-1}$  belonged to the monoclinic phase as in agreement with the previous report [37]. Thus, the Raman spectroscopic studies also confirmed that M-ZrO<sub>2</sub>-U-N has purely monoclinic phase whereas T-ZrO<sub>2</sub>-U-N has both tetragonal and monoclinic phases, as in line with the results obtained from XRD analysis.

## 2.3 Role of exposed facet and active sites in the catalyst

**Microscopic Analysis:** To shed light on the role of crystal facet and particle size, low and high-resolution TEM images for M-ZrO<sub>2</sub>-U-N and T-ZrO<sub>2</sub>-U-N nanoparticles were carefully captured and are shown in Figure 2. The TEM image of M-ZrO<sub>2</sub>-U-N (Figure 2a) displayed an average particle size of  $10 \pm 5$  nm, which is in good agreement with the particle size obtained from XRD by using the Scherrer equation (Table S1). The d-spacing values of M-ZrO<sub>2</sub>-U-N nanoparticles were measured through the HRTEM image (Figure 2b) and estimated to be 0.28, 0.31, and 0.36 nm, which corresponds to the crystal facets of (111), (-111) and (110) of monoclinic  $\text{ZrO}_2$  phase, respectively. Moreover, the analysis of Fast Fourier transform (FFT) pattern (inset in Figure 2b) obtained from the marked area confirmed the presence of (110), (111) and (-111) crystal facets in the M-ZrO<sub>2</sub>-U-N nanoparticles, implying that the nanoparticles are composed of



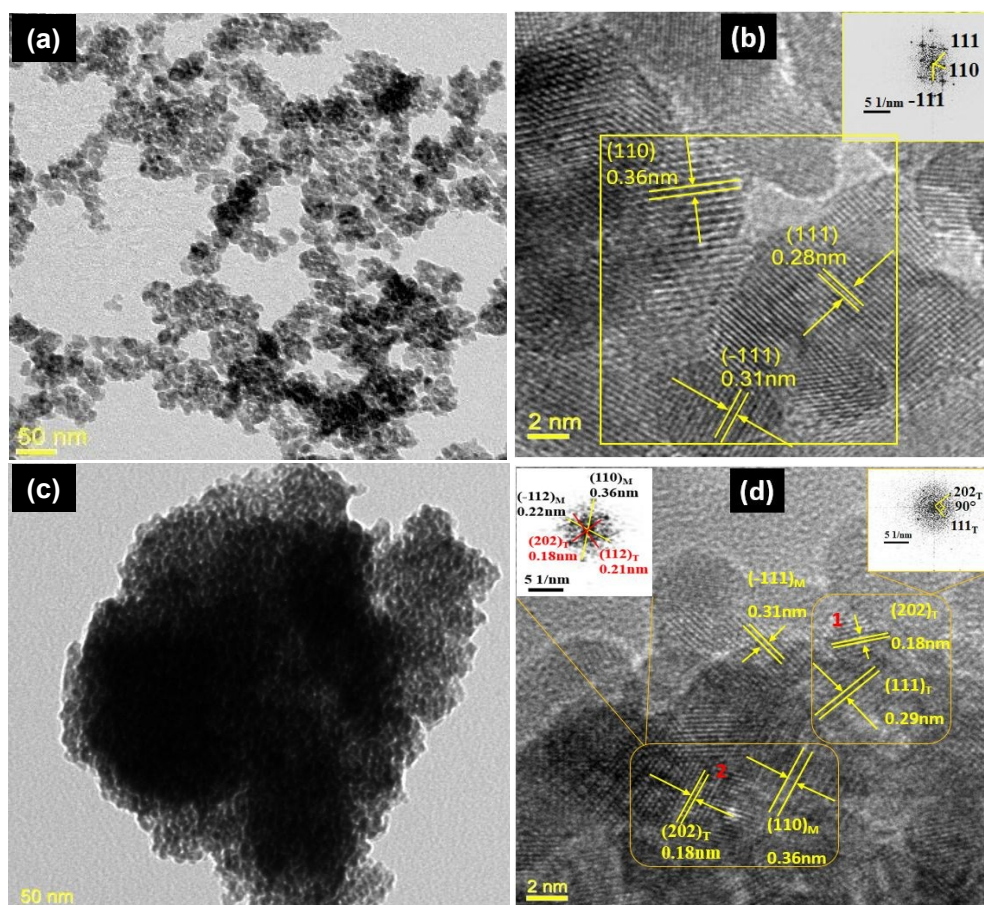


Figure  
resolution  
M-ZrO<sub>2</sub>-U-  
U-N

2. Low and high-  
TEM images of (a, b)  
N, and (c, d) T-ZrO<sub>2</sub>-  
nanoparticles

purely monoclinic ZrO<sub>2</sub> phase. Similarly, the average particle size of the T-ZrO<sub>2</sub>-U-N nanoparticles was found to be 20 nm (Figure 2c). The HRTEM image of T-ZrO<sub>2</sub>-U-N nanoparticles showed lattice fringes having d-spacing values of 0.18, 0.29, 0.31 and 0.36 nm (Figure 2d). According to the database of powder diffraction patterns (JCPDS# 00-017-0923), the pure tetragonal phase of ZrO<sub>2</sub> can have a maximum d-spacing value of 0.29 nm, corresponding to (111) plane. Therefore, the observed d-spacing value of 0.18 and 0.29 nm can be attributed to the (220) and (111) crystal facets of tetragonal ZrO<sub>2</sub> whereas 0.31 and 0.36 nm correspond to the (-111) and (110) of monoclinic ZrO<sub>2</sub> (JCPDS # 00-037-1484), respectively. These observations were further confirmed with the FFT patterns obtained from the marked areas of the HRTEM image (Figure 2d). The analysis of the FFT pattern obtained from the marked area (inset on the upper-right side of Figure 2d) displayed the diffraction pattern corresponding to tetragonal ZrO<sub>2</sub> whereas that of marked area (inset on the upper-left side of Figure 2d) showed both tetragonal and monoclinic ZrO<sub>2</sub>. Hence, the detailed TEM analysis corroborates the presence of entirely monoclinic phase in M-ZrO<sub>2</sub>-U-N, whereas T-ZrO<sub>2</sub>-U-N possess a combination of both monoclinic and tetragonal phase in nanoparticles, as consistent with the XRD and Raman results.

**Poisoning Studies:** To get a deeper insight into the role of active sites in M-ZrO<sub>2</sub>-U-N, systematic experiments were performed by adding an acid (2-nitrobenzoic acid) or a base (pyridine) additive to poison

Table 2: Influence of acid and base additives on the yield of FOH.

Entry	Catalyst	Additive	FFA Conv. (%)	FOH Yield (%)
1 <sup>a</sup>	M-ZrO <sub>2</sub> -U-N	Pyridine	86.8	73.8
2 <sup>b</sup>	M-ZrO <sub>2</sub> -U-N	2-Nitrobenzoic acid	8.3	1.4
3 <sup>c</sup>	-	Pyridine	0	0
4 <sup>d</sup>	-	2-Nitrobenzoic acid	12.4	0

Reaction conditions: 1 mmol FFA, 80 mg M-ZrO<sub>2</sub>-U-N catalyst, 4 ml isopropanol, 110 °C, 6 h. <sup>a</sup>80 mg pyridine added; <sup>b</sup>80 mg 2-nitrobenzoic acid added. <sup>c,d</sup> The reaction was performed with 80 mg of pyridine or 2-nitrobenzoic acid in the absence of a catalyst.

the respective basic and acidic sites of catalyst during the reaction, and the results are summarized in Table 2. It has been previously reported that Zr<sup>4+</sup> and O<sup>2-</sup> ions of ZrO<sub>2</sub> contribute to weaker Lewis acidic sites and strong basic sites, respectively [39]. M-ZrO<sub>2</sub>-U-N gave a very good yield of FOH (73.8%) at a conversion of 86.8% FFA (Table 2, entry 1) when adding pyridine, which selectively passivates acidic

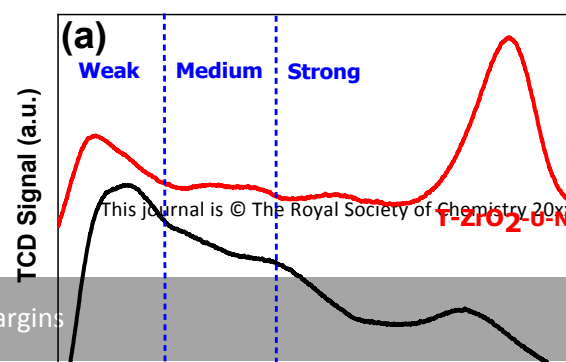


Figure 3. (a) CO<sub>2</sub>-TPD profile, (b, c) Zr3d and O1s XPS spectra and (d) AES spectra of M-ZrO<sub>2</sub>-U-N and T-ZrO<sub>2</sub>-U-N.

sites during the reaction, thus making basic sites freely available for catalysing the reaction. On the other hand, no significant yield of FOH (1.4%) with 8.0% conversion of FFA (Table 2, entry 2) was obtained with M-ZrO<sub>2</sub>-U-N when adding 2-nitrobenzoic acid, which selectively prevents the basic sites, thus enabling acidic sites unhampered for catalysing the reaction. When using pyridine and 2-nitrobenzoic acid as catalyst separately in the absence of M-ZrO<sub>2</sub>-U-N, no FOH was formed, indicating no catalytic role of these additives on FOH formation. These experimental results demonstrated that basic sites in M-ZrO<sub>2</sub>-U-N virtually uniquely participated in catalysing FFA to FOH in isopropanol (Table 2, entry 3 and 4).

**CO<sub>2</sub>-TPD Analysis:** To corroborate further the role of basic sites, M-ZrO<sub>2</sub>-U-N and T-ZrO<sub>2</sub>-U-N were subjected to CO<sub>2</sub>-temperature programmed desorption (CO<sub>2</sub>-TPD) analysis and the corresponding profiles are given in Figure 3a. M-ZrO<sub>2</sub>-U-N possessed total basic sites of 521 μmol/g, which is more than 2.2-fold higher than that obtained for T-ZrO<sub>2</sub>-U-N (238 μmol/g). Moreover, the weak (50-200 °C), medium (200-350 °C) and strong (350-750 °C) basic sites were also quantified and found that M-ZrO<sub>2</sub>-U-N contained 2-fold higher

medium and strong basic sites in total than T-ZrO<sub>2</sub>-U-N [40]. The basic sites have been divided into three kinds such as weak, medium and strong based on previously reported articles<sup>[40]</sup>. It has been generally considered that desorption temperature below 200 °C belongs to the weak basic sites and above 200 °C regarded as medium and strong basic sites. Furthermore, M-ZrO<sub>2</sub>-U-N possessed 4.4-times higher medium sites than T-ZrO<sub>2</sub>-U-N. The results obtained from CO<sub>2</sub>-TPD analysis indicate that medium and strong basic sites present in M-ZrO<sub>2</sub>-U-N played a crucial role in catalysing the transformation of FFA to FOH (89.8%) with a selectivity of 97.1% (Table 1, entry 3). On the other hand, T-ZrO<sub>2</sub>-U-N yielded only 8.1% FOH with a selectivity of 36.4% (Table 1, entry 4). Similarly, the CO<sub>2</sub>-TPD profiles of other catalysts (M-ZrO<sub>2</sub>-U-C, T-ZrO<sub>2</sub>-U-C and ZrO<sub>2</sub>-C) and their weak, medium and strong basic sites are presented in Figure S3 and Table S3, respectively. Moreover, the strong basic sites peak appeared at 650 °C for M-ZrO<sub>2</sub>-U-N might have predominantly contributed to the active basic sites compared to the peak appeared at 600 °C in the case of T-ZrO<sub>2</sub>-U-N, which showed an inferior activity (Figure 3a). Concurrently, T-ZrO<sub>2</sub>-U-N possessed a very low ratio of (-111/111) facet (Table S2) and exhibited a poor activity, even though, T-ZrO<sub>2</sub>-U-N displayed a major peak around 600 °C. Furthermore, the peak appeared at 600 °C for strong basic sites from T-ZrO<sub>2</sub>-U-N might have originated from (111) facet of ZrO<sub>2</sub>, which could be less active for this hydrogenation reaction. Similarly, M-ZrO<sub>2</sub>-U-C also displayed

a peak around 650 °C and showed comparable catalytic activity to M-ZrO<sub>2</sub>-U-N (Table 1 and Figure S3), implying that strong basic sites might have originated from (-111) facet of ZrO<sub>2</sub>. These results further manifest that the higher the medium and strong basic sites in total, the higher the conversion to FOH.

**XPS Analysis:** To get more insight with regard to the chemical states as well as the acidic and basic sites, M-ZrO<sub>2</sub>-U-N and T-ZrO<sub>2</sub>-U-N were subjected to X-ray photoelectron spectroscopy (XPS) analysis, and the corresponding spectra are shown in Figure 3b and c. The XPS spectrum of M-ZrO<sub>2</sub>-U-N (Figure 3b) showed two peaks at 181.8 and 184.2 eV, which can be assigned to the respective Zr 3d5/2 and Zr 3d3/2 lines. These lines indicate the presence of Zr<sup>4+</sup> species, implying that M-ZrO<sub>2</sub>-U-N is composed of ZrO<sub>2</sub> [36]. Similarly, the XPS spectrum of T-ZrO<sub>2</sub>-U-N (Figure 3b) also indicates the presence of Zr<sup>4+</sup> species; however, the peak positions of Zr 3d5/2 (182.0 eV) and Zr 3d3/2 (184.4) lines slightly shifted towards higher binding energy values in comparison to that of M-ZrO<sub>2</sub>-U-N (181.8 and 184.2 eV), inferring that T-ZrO<sub>2</sub>-U-N possibly contained more Lewis acidic sites [41]. In other words, M-ZrO<sub>2</sub>-U-N possesses more basic sites, which is consistent with the results obtained from CO<sub>2</sub>-TPD. Concomitantly, O1s spectra of both M-ZrO<sub>2</sub>-U-N and T-ZrO<sub>2</sub>-U-N were also obtained through XPS analysis to find out the chemical states of oxygen species and found to be not symmetrical in shape. Thus, the peaks were deconvoluted and are shown in Figure 3c. The spectra of both M-ZrO<sub>2</sub>-U-N and T-ZrO<sub>2</sub>-U-N exhibit two peaks at 529.7 and 531.2 eV, which can be attributed to the lattice (O<sub>latt</sub>) and adsorbed oxygen (O<sub>ads</sub>), respectively [42]. In order to calculate the surface oxygen concentration, the relative ratio of O<sub>ads</sub>/O<sub>latt</sub> was calculated based on the area under the peak. The calculated O<sub>ads</sub>/O<sub>latt</sub> in M-ZrO<sub>2</sub>-U-N was found to be 32% whereas 40 % for that of T-ZrO<sub>2</sub>-U-N. On the other way around, M-ZrO<sub>2</sub>-U-N contains 68% of lattice oxygen species which is 8% higher than that of T-ZrO<sub>2</sub>-U-N, indicating that M-ZrO<sub>2</sub>-U-N have relatively more exposed lattice oxygen species which contributes to the basic sites [43].

**AES Analysis:** To further quantify and substantiate the surface oxygen concentration, M-ZrO<sub>2</sub>-U-N and T-ZrO<sub>2</sub>-U-N were carefully analyzed through Auger electron spectroscopy (AES) and the corresponding spectra are shown in Figure 3d. Four similar characteristic peaks at 90, 141, 149 and 511 eV were observed for M-ZrO<sub>2</sub>-U-N, which can be assigned to Zr(MNN)metal, Zr(MNV)oxide, Zr(MNV)metal and O(KLL), respectively, according to the reported literature [44, 45]. Similarly, very slightly lowered kinetic energy values were observed for T-ZrO<sub>2</sub>-U-N (Figure 3d). The surface oxygen concentration (Co) of each catalyst was calculated based on the equation given below, employing the peak intensities of Zr(MNV)metal and O(KLL) [44].

$$Co = \frac{I_o / S_o}{\sum_j I_j / S_j}$$

where  $I_j$  and  $S_j$  represent the intensities and sensitivity factors of the  $j^{\text{th}}$  peak, respectively. The sensitivity factor of 0.5 and 0.22 for O (KLL) and Zr(MNV)metal peaks were employed for the calculation according to reported literature [44]. The calculated Co of M-ZrO<sub>2</sub>-U-N and T-ZrO<sub>2</sub>-U-N was found to be 89 and 73%, respectively, suggesting that M-ZrO<sub>2</sub>-U-N has a relatively larger number of basic

sites than that of T-ZrO<sub>2</sub>-U-N, which is in good agreement with CO<sub>2</sub>-TPD results.

DOI: 10.1039/D0CY01259A

**Plausible reaction mechanism:** On the basis of the results obtained from various characterizations through XRD, TEM, CO<sub>2</sub>-TPD, XPS and AES, and the poisoning studies, one can understand that M-ZrO<sub>2</sub>-U-N having purely monoclinic crystal phase with highest basic sites among employed catalysts played a crucial role in the transformation of FFA to FOH reaction. The following plausible reaction mechanisms (pathway 1 and 2) for the transformation of FFA to FOH with M-ZrO<sub>2</sub>-U-N are proposed and shown in Figure 4. The mechanism of pathway 1 proceeds through three key steps viz., i) interaction between isopropanol and the basic sites (O of ZrO<sub>2</sub>) of M-ZrO<sub>2</sub>-U-N to form four-membered cyclic intermediate state [46], ii) FFA interaction with acidic sites (Zr) of M-ZrO<sub>2</sub>-U-N, consequently, forming six-membered cyclic intermediate thereby hydride transfer takes place and iii) finally desorption of FOH from the surface of M-ZrO<sub>2</sub>-U-N, resulting in the regeneration of M-ZrO<sub>2</sub>-U-N for next catalytic cycle [47]. In case of pathway 2, when adding 2-nitrobenzoic acid as an additive to passivate the basic sites of M-ZrO<sub>2</sub>-U-N by absorbing a proton from the acid additive, the initial adsorption of isopropanol on the basic sites of M-ZrO<sub>2</sub>-U-N was hampered, forming negligible amount of FOH (pathway 2, Figure 4) (entry 2, Table 2). From the above mechanistic pathway, one could understand that the adsorption of isopropanol over the basic sites of M-ZrO<sub>2</sub>-U-N was the crucial step.

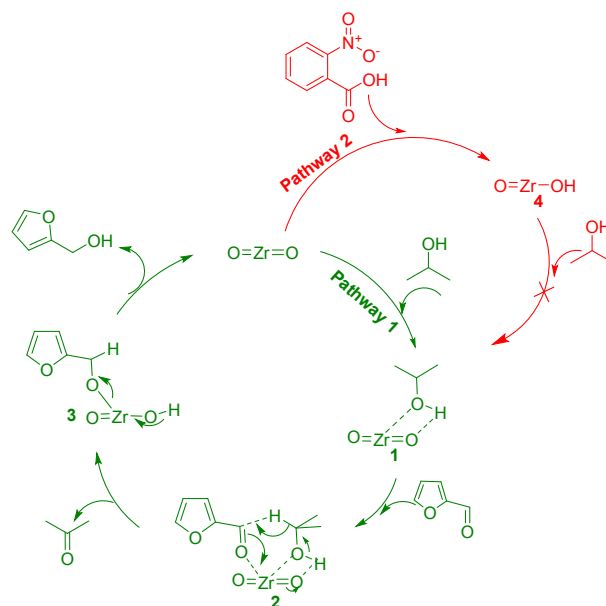




Figure 4. Plausible mechanistic pathways for the conversion of FFA to FOH with M-ZrO<sub>2</sub>-U-N in the absence and presence of the acid additive.

## 2.4 Activity of various ZrO<sub>2</sub> at similar conversion

To determine the real activity of various ZrO<sub>2</sub> catalysts, it is very imperative to compare the relative catalytic activities at a similar conversion of FFA under identical reaction conditions. With regard to this, the experiments were performed to obtain a conversion range of 30-50% of FFA, and the results are presented in Table 3. The reaction with M-ZrO<sub>2</sub>-U-N afforded 33.4 % conversion of FFA with FOH selectivity of 94.9% after 30 min of reaction time (Table 3, entry 3), whereas T-ZrO<sub>2</sub>-U-N required 24 h of reaction time to achieve 40.7% conversion with FOH yield of only 26.7% (Table 3, entry 4). Moreover, turn over frequency (TOF) of M-ZrO<sub>2</sub>-U-N and T-ZrO<sub>2</sub>-U-N were also calculated based on total basic sites obtained from CO<sub>2</sub>-TPD and found to be 15.1 and 0.57 h<sup>-1</sup>, respectively, manifesting that

monoclinic crystal phase of M-ZrO<sub>2</sub>-U-N has 27-fold higher catalytic activity than that of the tetragonal crystal phase of T-ZrO<sub>2</sub>-U-N.

The initial rate of all the catalysts based on their surface area was also calculated and are presented in Table 3. M-ZrO<sub>2</sub>-U-N possessed a higher initial rate of 69.6 μmolm<sup>-2</sup>h<sup>-1</sup> than that of all the other catalyst (Table 1 and 3). Moreover, M-ZrO<sub>2</sub>-U-N has a higher surface area and pore volume, which could contribute to the reaction on enhancing the yield of FOH. Unpromisingly, the ZrO<sub>2</sub>-C showed negligible activity in terms of FOH yield (2.2%) with an initial rate of 0.03 μmolm<sup>-2</sup>h<sup>-1</sup> even after a prolonged reaction time of 96 h (entry 5, Table 3). with M-ZrO<sub>2</sub>-U-N (Table 3).

Similarly, the results obtained with other catalysts (M-ZrO<sub>2</sub>-U-C and T-ZrO<sub>2</sub>-U-C) showed moderate activities in comparison that M-ZrO<sub>2</sub>-U-N. Overall, it can be concluded showed a highest catalytic activity in terms of FOH yield with the highest selectivity, owing to the prominent role of (-111) crystal facet possessing a maximum number of basic sites with a substantial amount of exposed lattice oxygen species along with high surface area and pore volume.

Table 3: The activity of different ZrO<sub>2</sub> catalysts similar conversion

Entry	Catalyst	FOH Yield [%]	Sel. <sup>a</sup> [%]	Time [h]	Surface Area [m <sup>2</sup> g <sup>-1</sup> ]	Pore Volume [cm <sup>3</sup> g <sup>-1</sup> ]	Total Basic Sites [μmolg <sup>-1</sup> ]	Initial Rate <sup>b</sup> [μmolm <sup>-2</sup> h <sup>-1</sup> ]	TOF <sup>c</sup> [h <sup>-1</sup> ]
1	M-ZrO <sub>2</sub> -U-C	17.8	43.9	0.5	106.9	0.23	433	41.6	10.2
2	T-ZrO <sub>2</sub> -U-C	36.6	74.5	4	70.4	0.04	311	16.2	3.6
3	M-ZrO <sub>2</sub> -U-N	31.7	94.9	0.5	113.9	0.26	524	69.6	15.1
4	T-ZrO <sub>2</sub> -U-N	26.7	65.6	24	49.3	0.04	241	2.8	0.57
5	ZrO <sub>2</sub> -C	2.2	10.5	96	25.6	0.03	19	0.11	0.15

Reaction conditions: 1 mmol FFA, 80 mg catalyst, 4 ml isopropanol, 110 °C, <sup>a</sup> Selectivity= yield/conversion, <sup>b</sup> Initial rate= (FOH mol)/ (BET surface area\* catalyst weight time\*time), <sup>c</sup> TOF= (FOH mol)/ (basic sites\*catalyst weight\*time)

## 2.5 Influence of other reaction parameters on the yield of FOH

The influence of reaction parameters such as temperature, time and catalyst loading was also optimised with the best efficient catalyst (M-ZrO<sub>2</sub>-U-N), and the results are shown in Figure S4. The results revealed that as the reaction temperature increases from 75 to 125 °C, the conversion of FFA and the yield of FOH increases from 53.6 to 99% and 35.2 to 99%, respectively (Figure S4a). In the cases of reaction time and catalyst loading, a similar trend of increase in both the conversion of FFA and formation of FOH was observed with longer reaction time (Figure S4b) and higher amount of catalyst loading (Figure S4c). The stability of M-ZrO<sub>2</sub>-U-N was also studied by treating the catalyst with isopropanol as a solvent in ace pressure tube at 110 °C for 24 h, followed by drying at 80 °C and tested its activity towards the conversion of FFA to FOH in fresh isopropanol at 110 °C for 6 h. The obtained result revealed that the catalytic activity of treated M-ZrO<sub>2</sub>-U-N remained unchanged in comparison with the

untreated M-ZrO<sub>2</sub>-U-N, indicating that the catalyst was quite stable during the reaction. In a similar fashion, the stability of FOH was also studied in isopropanol in the presence of M-ZrO<sub>2</sub>-U-N at 110 °C for 6 h and the obtained results based on Gas Chromatography (GC) analysis revealed that there was no significant degradation of FOH, implying that the final product FOH during the reaction was also very stable.

## 2.6. Kinetic study and hydrogenation of other bio-based substrates

The kinetic study of catalyst for the transformation of FFA to FOH was also performed with M-ZrO<sub>2</sub>-U-N at various temperature (348 to 398 K) and time (30 to 360 min), and the results are shown in Table S4 and Figure S5. According to the previous study, the transformation of FFA to FOH follows the first-order rate-law, that is,  $-\ln(1-x)=kt$ , where  $x$ ,  $k$  and  $t$  are the FFA conversion, rate constant and reaction time, respectively [33]. Therefore, the rate constant ( $k$ ) of each



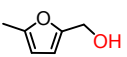
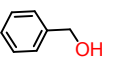
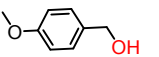
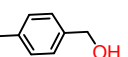
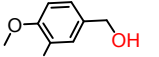
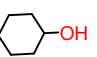
## ARTICLE

## Journal Name

reaction at a different time and temperature was calculated by plotting the graphs of  $-\ln(1-x)$  vs  $t$  and the obtained results are summarised in Table S4. Further, the activation energy was also calculated using the Arrhenius equation and found to be  $49 \text{ kJ/mol}^{-1}$  (Table S5), which is 1.2 to 1.3 times lower than that of previously reported catalysts (ZrPN,  $\text{ZrO}_2$  and Zr-beta) [33,48]. These results demonstrate that M-ZrO<sub>2</sub>-U-N showed an excellent catalytic activity among all the reported catalysts, owing to the presence of predominantly exposed (-111) crystal facet having a large number of basic sites along with high surface area and pore volume, which facilitated the facile adsorption of FFA followed by hydrogenation to FOH in isopropanol.

The activity of M-ZrO<sub>2</sub>-U-N was extrapolated for hydrogenation of other bio-based carbonyl compounds (5-methylfurfural, benzaldehyde, anisaldehyde, p-tolualdehyde, veratraldehyde and cyclohexanone) under similar reaction conditions, and the results are presented in Table 4. The yields of corresponding alcohols were obtained between 77.0 and 100% at reaction condition of  $110^\circ\text{C}$  for 6-10 h depending on the reactivity of the substrate. High conversion of these aldehydes and ketone to the corresponding alcohols with the better yields were achieved with M-ZrO<sub>2</sub>-U-N at a relatively lower temperature as compared to the reported zirconium nanohybrid catalyst [33]. For example, with zirconium nanohybrid, benzaldehyde conversion to benzyl alcohol required a reaction temperature of  $160^\circ\text{C}$  temperature for 6 h, whereas M-ZrO<sub>2</sub>-U-N needed relatively a low temperature ( $110^\circ\text{C}$ ), demonstrating that M-ZrO<sub>2</sub>-U-N possesses active basic sites in (-111) crystal facet, which could efficiently catalyze the reaction at a relatively lower temperature.

Table 4: Hydrogenation of various bio-based carbonyl compounds with M-ZrO<sub>2</sub>-U-N.

$\text{R}-\text{C}(=\text{O})-\text{R}' \xrightarrow[\text{Iso-propanol}]{\text{M-ZrO}_2\text{-U-N}} \text{R}-\text{CH}(\text{OH})-\text{R}'$	
 5-methylfurfural alcohol Y=97% (6h)	 Benzylalcohol Y=>99% (9h)
 (4-methoxyphenyl)methanol Y=99.9% (9h)	 p-tolylmethanol Y=99% (9h)
 Veratrole alcohol Y=77% (9h)	 Cyclohexanol Y=98% (6h)

Reaction conditions: 1 mmol substrate, 80 mg M-ZrO<sub>2</sub>-U-N, 4 ml isopropanol,  $110^\circ\text{C}$ .

## 2.7 Recyclability of M-ZrO<sub>2</sub>-U-N

The recyclability of M-ZrO<sub>2</sub>-U-N for the conversion FFA to FOH was studied at lower conversion (<30.0%) in isopropanol for four runs and the results are shown in Figure 5. After each run, the spent M-ZrO<sub>2</sub>-U-N was employed after recovering by washing with ethanol and acetone and dried at  $80^\circ\text{C}$  overnight followed by calcination at  $400^\circ\text{C}$  for 6 h in air. After the first run, 25.0% of FOH with 26.7% conversion of FFA was obtained. The activity of recovered M-ZrO<sub>2</sub>-U-N was slightly lost in the second run, yielding 21.0% FOH, suggesting that organic moieties might have strongly adsorbed on the active sites. After the third run, no significant loss in activity was found and maintained the yield of FOH about 18.0%. Furthermore, the comparison of the XRD pattern (Figure S6) obtained from the recovered after the fourth run and the fresh M-ZrO<sub>2</sub>-U-N revealed that the crystal structure or composition remains unchanged. However, the ratio of exposed surface facet between (-111) to (111) was found to be 1.34, which is slightly lower than that of fresh catalyst (1.51), confirming the active participation of (-111) facet in the reaction. The slight decrease in the activity of M-ZrO<sub>2</sub>-U-N during the subsequent reactions of recyclability test was due to a slight loss in the amount of exposed (-111) facet.

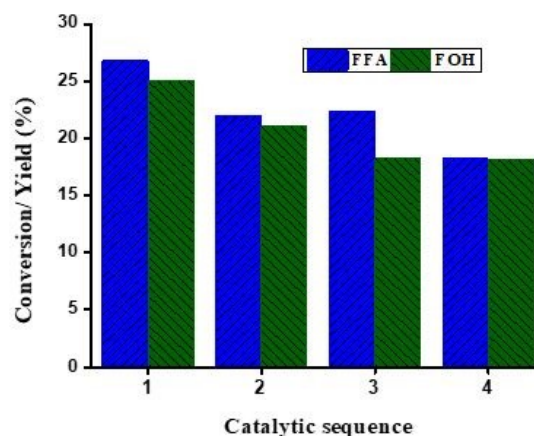


Figure 5. Recyclability of M-ZrO<sub>2</sub>-U-N for the conversion of FFA to FOH. Reaction conditions: M-ZrO<sub>2</sub>-U-N to furfural ratio = 1.20, isopropanol to furfural ratio = 32.7,  $110^\circ\text{C}$ , 30 min.

## 3. Conclusions

In summary, we have demonstrated the successful preparation of various ZrO<sub>2</sub> based catalysts for the transformation of FFA to FOH in isopropanol. Among all the catalyst, M-ZrO<sub>2</sub>-U-N showed an excellent activity with a maximum yield of FOH (99.9%). Based on the detailed analysis of XRD and TEM, it was revealed that M-ZrO<sub>2</sub>-U-N possesses purely monoclinic phase while the least active catalyst, T-ZrO<sub>2</sub>-U-N (8.1% FOH) has predominantly tetragonal phase along with minimal amount of monoclinic phase, inferring that the monoclinic phase of M-ZrO<sub>2</sub>-U-N is responsible for the efficient transformation of FFA to FOH. Among the synthesized catalysts, two catalysts (M-ZrO<sub>2</sub>-U-N and M-ZrO<sub>2</sub>-U-C) exhibit purely monoclinic phase, however, M-ZrO<sub>2</sub>-U-N displayed the best catalytic activity in terms of product formation and selectivity, owing to the presence of more exposed (-111) crystal facet in comparison to that of M-ZrO<sub>2</sub>-U-C. Insight studies related to the poisoning of acidic and basic sites

present in the monoclinic phase of M-ZrO<sub>2</sub>-U-N with pyridine or 2-nitrobenzoic acid additives during the reaction untangled that basic sites in the catalyst play a critical role on the yield of FOH. Moreover, CO<sub>2</sub>-TPD, XPS and AES analysis also confirmed the presence of the highest basic sites and exposed surface oxygen concentration in M-ZrO<sub>2</sub>-U-N among all the catalysts. In addition to the monoclinic phase, surface oxygen species and basic sites, the higher surface area and pore volume of M-ZrO<sub>2</sub>-U-N also contributed to the reaction on enhancing the yield of FOH. The kinetic studies also revealed that M-ZrO<sub>2</sub>-U-N requires low activation barrier of 49.0 kJmol<sup>-1</sup> for the FFA conversion reaction in comparison with that of the previously reported zirconium-based catalysts, which could be due to the presence of active basic sites on the exposed (-111) facet of M-ZrO<sub>2</sub>-U-N. M-ZrO<sub>2</sub>-U-N was possible to reuse at least for three times with a minimal loss of activity, and could efficiently convert other bio-based aldehydes and ketone in excellent yields (77-99.9%), paving the way for transforming a wide range of biomass based carbonyl compounds to their corresponding alcohols.

## 4. Experimental

### 4.1 Chemicals

Furfural, furfuryl alcohol, naphthalene, zirconium oxynitrate hydrate, zirconium oxychloride octahydrate, 5-methyl furfural, cyclohexanone, benzaldehyde, p-touladehyde, anisaldehyde, veratraldehyde, veratryl alcohol, 5-methyl-2-furyl methanol, benzyl alcohol, cyclohexanol, pyridine and 2-nitrobenzoic acid were purchased from Sigma Aldrich. Urea and Isopropanol were bought from TCI chemicals respectively. All the chemicals are of analytical grade and used without any further treatment or purification.

### 4.2 Catalyst preparation

All the ZrO<sub>2</sub> based catalysts were prepared by slightly modifying the procedure available in the previous report [37]. In a typical synthesis, 0.4 mol of zirconium precursor (zirconium oxynitrate/zirconium oxychloride) and 2 mol of the precipitating agent (urea) were dissolved in 30 mL of solvent (methanol/distilled water). The solution was then transferred to Teflon lined autoclave of 100 ml capacity and placed in an oven at 140 °C for 20 h after completely sealed. After each reaction, the autoclave was naturally cooled down to room temperature and each catalyst was thoroughly washed with distilled water and methanol and dried at 100 °C. Subsequently, each catalyst was calcined at 400 °C for 4 h with a ramp rate of 2 °C/min in atmospheric air to obtain the final catalyst for the reactions. For the catalysts; T-ZrO<sub>2</sub>-U-N and T-ZrO<sub>2</sub>-U-C, zirconium oxynitrate and zirconium oxychloride were used as respective Zr precursors while methanol and urea were utilized as a solvent and precipitating agent. On the other hand, M-ZrO<sub>2</sub>-U-N and M-ZrO<sub>2</sub>-U-C were also prepared using zirconium oxynitrate and zirconium oxychloride as their respective Zr precursors with water and urea. ZrO<sub>2</sub>-C was derived from commercialized ZrO<sub>2</sub> (obtained from Sigma-Aldrich) by calcining at 400 °C for 4 h with a ramp rate of 2 °C/min and atmospheric condition.

### 4.3 Characterisation Techniques

View Article Online  
DOI: 10.1039/D0CY01259A

The phase identification and purity of all the catalysts were determined in the 2θ range of 20-80° at a scan rate of 2°/min through powder X-ray diffractometer (PANalytical Xpert Pro. equipped with X'Celerator solid-state detector at the operating parameter of the 45 kV, 40 mA, with target Cu-Kα (λ= 1.54056 Å). The Raman spectra were recorded in the range of 100-1500 cm<sup>-1</sup> using Raman spectroscopy (BWTEK Inc.) at an excitation wavelength of 532 nm. The average particle size and lattice spacing of the catalysts; M-ZrO<sub>2</sub>-U-N and T-ZrO<sub>2</sub>-U-N were examined through transmission electron microscopy (TEM, FEI Tecnai) at operating voltage of 200 keV. The chemical states and the surface oxygen concentration of M-ZrO<sub>2</sub>-U-N and T-ZrO<sub>2</sub>-U-N were also measured through X-ray photoelectron and Auger electron spectroscopy (PHI 5000 versa Prob II, FEI Inc.) in a binding or kinetic energy range of 0 to 1200 eV with monochromatic X-ray source of Al Kα. The instrument was priority calibrated with C1s at a binding energy of 284.6 eV. The number of basic sites in all the catalysts was also determined by CO<sub>2</sub>-temperature programmed desorption (CO<sub>2</sub>-TPD) (BELCAT II version p0.5.1.10) equipped with TCD detector. 50mg of the catalyst was taken in a quartz tube and heated from room temperature to 500 °C within 60 min of time under He gas flow of 50ml/min and continue degassed for another 50 min at the same condition. Then, the tube containing catalyst was cooled down to 50 °C and performed CO<sub>2</sub> adsorption study under the gas of 5% CO<sub>2</sub>-He at a flow rate of 50 ml/min. Subsequently, the catalyst was flushed with He gas at a flow rate of 50 ml/min to remove physisorbed CO<sub>2</sub>. Finally, desorption studies were carried out at a temperature range of 50-750 °C at the ramp rate of 10 °C/min. The surface areas and pore volumes of all the catalysts were determined from N<sub>2</sub>-sorption measurement at liquid nitrogen temperature through BET and t-plot methods, respectively, using a Quantachrome Nova 2000e/Micromeritics ASAP 2020 physisorption analyzer. Each sample was degassed at 150 ° for 6 h under vacuum prior to the analysis.

### 4.4 Catalytic reactions

All the reactions were performed in a 15 ml ace pressure tube. In a typical reaction, 1mmol of FFA, 4 ml of isopropanol, 80 mg of catalyst and 15 mg of Naphtalene was taken in ace pressure tube and after tightly closed the pressure tube, it was dipped into a preheated silicon oil bath, which is already placed on a magnetic stirrer with a heating plate. The internal reaction temperature was measured using an ace pressure tube attached with a plunger valve and thermowell. After the completion of each reaction, the pressure tube was cooled down to room temperature naturally. An aliquot of each reaction mixture was withdrawn and filtered off using 0.2µm nylon syringe filter and analysed using Agilent 7890B gas chromatogram, equipped with flame ionization detector (FID) and DB-5 MS column (30m×0.32×0.25µm). The conversion of FFA and yield of FOH were quantified by making a series of individual standards along with naphthalene as an internal standard.

### Conflicts of interest

## ARTICLE

## Journal Name

The authors declare no competing financial interest.

## Acknowledgements

We gratefully thank the Department of Biotechnology (DBT), New Delhi, India, for the financial support and infrastructural facilities provided at CIAB. SK gratefully thanks CIAB/DBT for providing financial support through Senior Research Fellowship and Panjab University for PhD registration. We also acknowledge the National Agri-Food Biotechnology Institute for kindly permitting us to use GC. We thank SKK for allowing us to use BET surface area analyzer available at his laboratory at Panjab University.

## References

- (a) A. Corma, S. Iborra, A. Veltey, *Chem. Rev.* 2007, **107**, 2411-2502. (b) P. Gallezot, *Chem. Soc. Rev.* 2012, **41**, 1538-1558.
- (a) A. Sheldon, *Green Chem.* 2014, **16**, 950-963. (b) M. Chatterjee, T. Ishizaka, H. Kawanami, *Green Chem.* 2018, **20**, 2345. (c) A. J. Ragauskas, C. K. Williams, H. B. Davison, G. Britovsek, J. Cairney, C. A. Eckert, W. J. F. Jr, J. P. Hallett, D. J. Leak, C. L. Liotta, J. R. Mielenz, R. Murphy, R. Templer, T. Tschaplinski, *Science* 2006, **311**, 484-489. (d) M. S. Holm, S. Saravanamurugan, E. Taarning, *Science* 2010, **328**, 602-605.
- (a) W. R. Brode, R. W. V. Dolah, *Ind. Eng. Chem.* 1947, **39**, 1157-1160. (b) I. Mcmanus, H. Daly, J. M. Thompson, E. Connor, C. Hardacre, S. K. Wilkinson, N. S. Bonab, J. T. Dam, M. J. H. Simmons, E. H. Stitt, C. D. Agostino, J. McGregor, L. F. Gladdan, J. J. Delgado, *J. Catal.* 2015, **330**, 344-353. (c) R. L. Augustine, *Catal. Today* 1997, **37**, 419-440.
- (a) D. Lei, K. Yu, M. R. Li, Y. Wang, Q. Wang, T. Liu, P. Liu, L. L. Lou, G. Wang, S. Liu, *ACS Catal.* 2017, **7**, 421-432. (b) G. S. Zhang, M. M. Zhu, Q. Zhang, Y. M. Liu, H. Y. He, Y. Cao, *Green Chem.* 2016, **18**, 2155-2164.
- (a) A. Marimuthu, J. Zhang, S. Linic, *Science* 2013, **339**, 1590-1593. (b) X. Liu, X. Ye, F. Bures, H. Liu, Z. Jiang, *Angew. Chem. Int. Ed.* 2015, **54**, 11443-11447. (c) R. H. Tunuguntla, R. Y. Henley, Y. C. Yao, T. A. Pham, M. Wanunu, A. Noy, *Science* 2017, **357**, 792-796.
- (a) M. M. Villaverde, N. M. Bertero, T. F. Garetto, A. J. Marchi, *Catal. Today* 2013, **213**, 87-92.
- K. Yan, G. Wu, T. Lafleur, C. Jarvis, *RENEW. SUST. ENERG. REV.* 2014, **38**, 663-676.
- C. K. P. Neeli, Y. M. Chung, W. S. Ahn, *ChemCatChem* 2017, **9**, 4570-4579.
- P. Puthiaraj, K. Kim, W. S. Ahn, *Catal. Today* 2019, **324**, 49-58.
- C. R. Baria, M. Isaacs, K. Wilson, A. G. Ruiz, I. R. Ramos, *Appl. Catal. A* 2018, **563**, 177-184.
- X. Liu, B. Zhang, B. Fei, X. Chen, J. Zhang, X. Mu, *Faraday Discuss.* 2017, **202**, 79-98.
- X. Chen, L. Zhang, B. Zhang, X. Guo, X. Mu, *Sci. Rep.* 2016, **6**, 28558.
- J. Chen, F. Lu, J. Zhang, W. Yu, F. Wang, J. Gao, J. Xu, *ChemCatChem* 2013, **5**, 2822-2826.
- S. Sitthisa, D. E. Resasco, *Catal. Lett.* 2011, **141**, 784-791.
- S. Tian, W. Gong, W. Chen, N. Lin, Y. Zhu, Q. Feng, Q. Xu, Q. Fu, C. Chen, J. Luo, W. Yan, H. Zhao, D. Wang, Y. Li, *ACS Catal.* 2019, **9**, 5223-5230.
- M. Ghashghaee, S. Sadjadi, S. Shirvani, V. Farzaneh, *Catal. Lett.* 2017, **2**, 318-327.
- A. Driscoll, T. Curtin, W. Y. Hernandez, P. V. D. Voort, J. J. Leahy, *Org. Process Res. Dev.* 2016, **20**, 1917-1929.
- S. Rodiansono, T. Khairi, N. I. Hara, S. Shimazu, *Catal. Sci. Technol.* 2012, **2**, 2139-2145.
- J. J. Musci, A. B. Merlo, M. L. Casella, *Catal. Today* 2017, **296**, 43-50.
- M. G. Dohade, P. L. Dhepe, *Green Chem.* 2017, **19**, 1144-1154.
- O. F. Aldosari, S. Iqbal, P. J. Miedziak, G. L. Brett, D. R. Jones, X. Liu, J. K. Edwards, D. J. Morgan, D. K. Knight, G. J. Hutchings, *Catal. Sci. Technol.* 2016, **6**, 234-242.
- H. Li, W. Zhao, S. Saravanamurugan, W. Dai, J. He, S. Meier, S. Yang, A. Riisager, *Communications Chemistry*, 2018, **32**.
- A. Boddien, B. Loges, F. Gartner, C. Torberg, K. Fumino, H. Junge, R. Ludwig, M. Beller, *J. Am. Chem. Soc.* 2010, **132**, 8924-8934.
- M. Chia, J. A. Dumesic, *Chem. Commun.* 2011, **47**, 12233-12235.
- M. M. Villaverde, T. F. Garetto, A. J. Marchi, *Catal. Commun.* 2015, **58**, 6-10.
- J. He, H. Li, A. Riisager, S. Yang, *ChemCatChem* 2018, **10**, 430-438.
- J. He, L. Schill, S. Yang, A. Riisager, *ACS Sustainable Chem. Eng.* 2018, **6**, 17220-17229.
- X. Meng, Y. Yang, L. Chen, M. Xu, X. Zhang, M. Wei, *ACS Catal.* 2019, **9**, 4226-4235.
- R. Ramos, A. F. Peixoto, B. I. Arias-Serrano, O. S. G. P. Soares, M. F. R. Pereira, D. Kubicka, C. Freire, *ChemCatChem* 2019.
- H. Li, A. Riisager, S. Saravanamurugan, A. Pandey, R. S. Sangwan, S. Yang, R. Luque, *ACS Catal.* 2018, 148-187.
- H. Li, S. Yang, S. Saravanamurugan, A. Riisager, *ACS Catal.* 2017, **7**, 3010-3029.
- G. D. Wilk, R. M. Wallace, J. M. Anthony, *J. Appl. Phys.* 2001, **89**, 5243-5275.
- H. Li, J. He, A. Riisager, S. Saravanamurugan, B. Song, S. Yang, *ACS Catal.* 2016, **6**, 7722-7727.
- H. Li, X. Liu, T. Yang, W. Zhao, S. Saravanamurugan, S. Yang, *ChemSusChem* 2017, **10**, 1761-1770.
- M. Ma, P. Hou, J. Cao, H. Liu, X. Yan, X. Xy, H. Yue, G. Tian, S. Feng, *Green Chem.* 2019, **21**, 5969-5979.
- J. Zhang, K. Dong, W. Luo, H. Guan, *ACS Omega* 2018, **3**, 6206-6216.
- W. Li, H. Huang, H. Li, W. Zhang, H. Liu, *Langmuir* 2008, **24**, 8358-8366.
- A. Kushwaha, M. Aslam, *J. APPL. PHYS.* 2012, **112**, 54316.
- S. Kouva, K. Honkala, L. Lefferts, J. Kanervo, *Catal. Sci. Technol.* 2015, **5**, 3473.
- (a) S. Han, D. Zhao, T. Otroshchenko, H. Lund, U. Bentrup, V. A. Kondratenko, N. Rockstroh, S. Bartling, D. E. Doronkin, J. D. Grunwaldt, U. Rodemerck, D. Linke, M. Gao, G. Jiang and E. V. Kondratenko, *ACS Catal.* 2020, **10**, 8933-8949. (b) J. Ren, C. Mebrahtu and R. Palkovits, *Catal. Sci. Technol.* 2020, **10**, 1902-1913. (c) Y. Liu,

Y. Wu, Z. Akhtamberdinova, X. Chen, G. Jiang and D. Liu.  
*ChemCatChem*, 2018, **10**, 4689-4698.

View Article Online  
DOI: 10.1039/D0CY01259A

41. H. J. M. Bosman, A. P. Pijpers, A. W. M. A. Jaspers, *J. Catal.* 1996, **161**, 551-559.

42. M. Zhang, J. Zhang, Y. Wu, J. Pan, Q. Zhang, Y. Tan, Y. Han, *Appl. Catal. B: Environ.* 2019, **244**, 427-437.

43. K. Pokrovski, T. K. Jung, A. T. Bell, *Langmuir* 2001, **17**, 4297-4303.

44. Y. Nishino, A. R. Krauss, Y. Lin, D. M. Gruen, *J. Nucl. Mater.* 1996, **228**, 346-353.

45. T. Tanabe, M. Tanaka, S. Imoto, *Surf. Sci.* 1987, **187**, 499-510.

46. A. Segawa, K. Taniya, Y. Ichihashi, S. Nishiyama, N. Yoshida, N. Okamoto, *Ind. Eng. Chem. Res.* 2018, **57**, 70-78.

47. M. Boronat, A. Corma, M. Renz, *J. Phys. Chem. B* 2006, **110**, 21168-21174

48. M. Koehle, R. F. Lobo, *Catal. Sci. Technol.* 2016, **6**, 3018-3026.

## Table of Contents (TOC)

